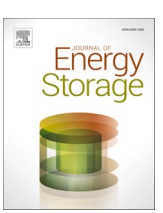
FISEVIER

Contents lists available at ScienceDirect

Journal of Energy Storage

journal homepage: www.elsevier.com/locate/est



Research Papers

NaI as suitable alkali halide hydrate for domestic thermochemical heat storage

Melian A.R. Blijlevens ^a, Ekaterina D. Garina ^a, Quirine D.K. Wildeman ^a, Roy van Alst ^a, Natalia Mazur ^{b,c,d}, Hugo Meekes ^a, Elias Vlieg ^{a,*}

- ^a Radboud University, Institute for Molecules and Materials, Heyendaalseweg 135, 6525 ED, Nijmegen, the Netherlands
- ^b TNO Materials Solutions, High Tech Campus 25, 5656 AE Eindhoven, the Netherlands
- ^c Department of Applied Physics, Eindhoven University of Technology, Den Dolech 2, 5600 MB Eindhoven, the Netherlands
- d Eindhoven Institute for Renewable Energy Systems, Eindhoven University of Technology, PO Box 513, 5600 MB Eindhoven, the Netherlands

ARTICLE INFO

Keywords: Thermochemical energy storage Salt hydrates Thermal analysis Hydration/dehydration Cycling

ABSTRACT

The limits and potentials of alkali (Li - Cs) halides (F - I) as salt hydrate-based thermochemical heat storage materials are studied. Most alkali halides are found unsuitable, and only the hydrates of sodium iodide (NaI) and sodium bromide (NaBr) were investigated experimentally. We confirmed that both have high energy densities of $1.5~\rm GJ/m^3$ and $1.6~\rm GJ/m^3$ respectively, based on the crystal structures of the dihydrate phases. NaI demonstrated full cyclic stability at water vapor pressures of 12 and 14.5 mbar, but NaBr did not show rehydration at these conditions. Therefore, NaBr was deemed unsuitable for domestic applications. For the NaI – H_2O system, we have measured the p,T equilibrium line between the hydration states and constructed p,T and T,x – phase diagrams. This showed that the hydration temperature is 42 °C for 12 mbar water vapor pressure which is enough for domestic space heating. Additionally, the phase diagrams revealed an incongruent melting point where the NaI- $2H_2O$ is in equilibrium with the anhydrate and a saturated aqueous NaI solution. This melting can overlap with dehydration and thereby hinders the cyclability, since in the melting process part of the salt is dissolved which blocks the pores formed during dehydration. Therefore, the performance of NaI can be improved by ensuring dehydration is completed below the incongruent melting point of 68 °C. We also found that pre-cycling can prevent deliquescence which is expected to occur at 25 °C and 12 mbar. Overall, NaI could be a candidate for low temperature heat storage.

1. Introduction

A paramount step in transitioning to renewable energy would be the use of a carbon-free source for heating houses, since in the domestic environment in the EU 80 % of the energy consumption is used for heating (space heating and hot tap water) [1]. A good source would be solar heat, because it is readily available and renewable. However, there is a seasonal mismatch in supply and demand which needs to be overcome. In order to solve this issue long-term heat storage is required. Currently a lot of research is going into thermochemical heat storage which is potentially suitable as a compact and long-term storage method. This method stores heat in a chemical reaction between a gas and a solid material to form a solvate. This makes it a thermochemical material (TCM) [2–6].

Donkers et al. [2] have presented a schematic overview of a TCM

reactor. Such a reactor consists of two compartments, connected with a valve; one contains the TCM and the other contains a solvent. The solvent can either be stored within the system (closed system) or externally supplied (open system) [2,7]. One disadvantage of an open system is that the TCM gets exposed to air with other potentially reactive gasses like $\rm O_2$ and $\rm CO_2$.

Salt hydrates have gained particular interest as TCMs since they have a high energy density and they use water as the solvent. Water vapor is the preferred gas in residential areas, because it is safe and readily available. The heat storage is then determined by the reaction heat of the reversible phase transition between different hydration states of the salt.

Potential salt hydrates have to fulfil a number of requirements to be of practical use in houses as formulated by Donkers et al. [2]. First of all, the salts are required to be readily available, non-toxic, chemically stable and have good energy density. The transition energy density

E-mail address: e.vlieg@science.ru.nl (E. Vlieg).

^{*} Corresponding author.

should preferably be larger than 1.3 GJ/m³ to limit the size of the storage system. In addition, the material has to dehydrate at a temperature below 150 °C, the maximum temperature which can be reached with solar collectors [6]. When we consider only space heating, the minimum required output temperature of our salt is 30 °C, since the input temperature is 25–30 °C for modern floor heating and we assume a small decrease in temperature due to sensible heat losses [8].

The water vapor pressure available during hydration is 12–15 mbar, limited by the lowest temperature of the system, which is set at 10 to 12 $^{\circ}C$ [2]. Therefore, the material should rehydrate at a minimum temperature of 30 $^{\circ}C$ at 12–15 mbar water vapor pressure.

For an overview of potential candidates, the reader is referred to references [2,4,5,9,10]. Among the candidates, alkaline earth halides are suggested frequently as thermochemical materials [2,6,11], but the only alkali halides previously referenced in the context of heat storage are LiCl $(1.83-2.08\,\text{GJ/m}^3)\,[2,12,13]$ and LiBr $(1.77-2.0\,\text{GJ/m}^3)\,[2,14]$. The other alkali halides are rarely mentioned. We therefore need to assess which alkali halides warrant further investigation based on the aforementioned availability, toxicity, stability, energy density and temperature requirements.

An overview of this assessment is given in Table 1, where all potential alkali halide hydration states are indicated with the respective numbers of water or "x" when there is no known hydrate. The salt hydrates are marked red when failing the requirements or green when they pass the initial assessment as elaborated in the following paragraph.

The lithium salts fail the availability requirement since lithium is a technology-critical element at risk of becoming scarce due to its use in electrical batteries [15]. Among the fluorides KF, RbF and CsF all form hydrates. Regrettably, these salts are highly toxic and chemically unstable [16-18], which makes them unsuitable for the domestic environment. This leaves only the hydrates of the sodium halides NaCl·2H₂O, NaBr·2H₂O and NaI·2H₂O. These salts are relatively safe. Only NaI has some risks with potentially causing skin irritation and being toxic to aquatic life [17,18]. Each of these salts has a theoretical energy density higher than 1.3 GJ/m³ namely, 1.9, 1.7 and 1.5 GJ/m³, respectively [19,20]. However, the temperature range requirement removes NaCl•2H₂O from the list since it only forms below 0.1 °C [21]. Finally, both NaBr·2H₂O and NaI·2H₂O remain, compounds that were already listed in the review of Donkers et al. [2], but that did not meet the requirement of having a hydration temperature above 50 °C needed for hot tap water. Nevertheless, they can be relevant for other applications like the aforementioned domestic space heating, which is still 63 % of the energy consumption in EU households [1]. Moreover, a combination with a heat pump could potentially make these salts applicable for hot tap water, because that would allow a large increase in water temperature with only a modest energy cost (because of the warm starting point).

A known disadvantage of NaI is that it is unstable in an aqueous solution when exposed to light and $O_2(g)$. The photooxidation of iodide ions (I⁻ (aq)) leads to formation of iodine (I₂ (aq)); the reaction pathway and mechanisms have been studied from the 1950s to 2000s [22–24].

Table 1 Overview of alkali halides and their ability to form hydrates [26–28]. If an alkali halide can form an "n" hydrate this is indicated with a number representing the possible hydration state(s), if no hydration states exist this is indicated with an "x". The salts marked red fail to meet the availability, toxicity, stability or temperature range requirements.

Alkali\Halide	F	Cl	Br	1
Li	х	1, 2, 3, 5	1, 2, 3, 5	1, 2, 3
Na	х	2	2	2
K	2, 4	х	х	х
Rb	1	х	х	х
Cs	1, 1.5	х	х	х

The complete reaction pathway, including a step mediated by O_2 (aq), is described by Watanabe et al. [25]. When applied as a TCM, this side-reaction can be avoided by working in a closed system (no exposure to light and O_2 -free).

The aim of this research is therefore to experimentally determine for NaBr and NaI whether they could be suitable as TCMs in domestic heat storage. For that, we first measured the energy densities to confirm the literature values, followed by a cyclability test with vapor pressures of 12–14.5 mbar. NaBr failed this test and thus only on NaI further experiments were done to determine the phase diagram and study the mechanism and the kinetics of the phase transformation.

2. Thermodynamics of the hydration states phase transition

The general equation for the reversible reaction between two hydration states of a salt MX in a water vapor environment can be written as:

$$MX \bullet nH_2O(s) \leftrightarrow MX \bullet mH_2O(s) + (n-m)H_2O(g),$$
 (1)

where removing the water molecules from the solid phase requires heat, while adding water molecules to the lower hydration state releases heat. In this paper M represents sodium and X is bromide or iodide. Within the relevant temperature range, these salts both have only two hydration states; the dihydrate (n=2) and the anhydrate (m=0). This leads to the thermodynamic equilibrium constant K determined by

$$\Delta_{r}G^{0} = -RTlnK = -RTln\frac{a(NaX(s)) \bullet a^{2}(H_{2}O(g))}{a(NaX \bullet 2H_{2}O(s))} = -2RTln\left(\frac{p}{p^{0}}\right),$$
(2)

where $\Delta_r G^0$ is the molar reaction Gibbs energy, R the gas constant, T the temperature in K, p is the water vapor pressure in mbar and p^0 is the standard pressure (1000 mbar). The activity a is set to one for the solids; we assume perfect gas behaviour for the vapor. Alternatively, the reaction Gibbs energy for dehydration at temperature T can be written as

$$\Delta_r G^0 = \Delta_r H^0 - T \Delta_r S^0. \tag{3}$$

In this equation, $\Delta_r H^0$ is the standard molar dehydration reaction enthalpy (J•mol⁻¹) and $\Delta_r S^0$ the standard molar dehydration reaction entropy (J•mol⁻¹•K⁻¹). Combining Eqs. (2) and (3) and assuming that $\Delta_r H^0$ is independent of the temperature, results in the linear form of the Van't Hoff equation,

$$2ln\left(\frac{p}{p^0}\right) = \frac{\Delta_r S^0}{R} - \left(\frac{\Delta_r H^0}{R}\right) \frac{1}{T}.$$
 (4)

When plotting $\ln(p)$ vs. 1/T, this equation can be used to estimate $\Delta_r H^0$ and $\Delta_r S^0$ per mole salt, and thus per 2 mol of water.

3. Materials and methods

3.1. Materials

NaI was supplied by Sigma-Aldrich (purity \geq 99.5 %) and by VWR chemicals (purity \geq 99 %) and NaBr by Sigma-Aldrich (purity 99–100.5 %).

3.2. Enthalpy determination

To determine the heat of transition for NaI and NaBr dihydrate to the anhydrate, dihydrate crystals of NaI and NaBr were grown by preparing a saturated solution in water at 50 $^{\circ}\text{C}$, followed by cooling at room temperature. The beaker with NaI solution was covered with aluminum foil to prevent photooxidation.

A sample of approximately 5 mg of dihydrate crystals was put in an aluminum 40 μ L pan with a pierced lid. This pan was put in a differential

scanning calorimeter (DSC) of type Mettler-Toledo DSC 3, where it was heated from $-10\,^{\circ}\text{C}$ to $90\,^{\circ}\text{C}$ with a heating rate of $0.1\,$ K/min. The heat of transition was determined by integrating the transition peak. This was then divided by the crystal volume of the dihydrate to calculate the energy density, following the practice in the literature to use the highest relevant hydrate as the reference state [2].

3.3. Thermogravimetric analysis

The NaI powder from the supplier was sieved prior to experiments using a Fritsch vibratory shaker and sieves of 100 and 150 μm to obtain a powder with a particle size range from 100 to 150 μm since in preliminary experiments this size distribution showed improved water vapor transport.

3.3.1. Cyclability measurements

A thermogravimetric analyzer (TGA) of type Mettler-Toledo TGA/ DSC 3+ was equipped with a humidity controller as described in our previous work [29]. Cyclability was tested by using approximately 10 mg of the sieved powder in a 100 µL pan without a lid. Starting with a dehydration step, each cycle consisted of dehydration for 4 h at 130 °C. followed by 6 h of hydration at 25 $^{\circ}$ C. Both the heating and cooling were done with a rate of 10 K/min. In a single experiment, ten of such cycles were measured. A follow-up experiment was done with an adapted heating rate of 0.1 K/min. The cooling rate was 10 K/min in all cyclability experiments. Throughout the experiment a constant water vapor pressure was applied as specified. As described in our previous work [29], the water vapor pressure was calibrated based on the deliquescence points of LiCl, CaBr2, MgCl2, CoBr2 and NaBr with an estimated error of ± 1.1 mbar. The airflow was slightly heated to prevent condensation in the set-up, since the sample pan was closest to the airflow the sample temperature was 27 °C during the hydration steps.

3.3.2. Metastable zone determination

Metastable zone (MSZ) values, i.e. the kinetic difference in transition temperature versus the equilibrium phase transition temperature, were measured for sieved NaI powder using TGA at a fixed water vapor pressure (12 or 22 mbar). The salt was first kept at 130 $^{\circ}\text{C}$ for 2 h followed by cooling with a rate of 0.1 K/min to 25 $^{\circ}\text{C}$. The sample remained at this temperature for 1.5 h, followed by heating to 130 $^{\circ}\text{C}$ once more with a heating rate of 0.1 K/min and was finally left at this temperature for 2 h. The MSZ was determined by measuring the onset temperatures of hydration or dehydration.

3.4. Phase transition measurements

A p,T-meter set-up as described by Sögütoglu et al. [30] was used to measure the equilibrium phase line of the NaI-H₂O system. Approximately 1 g of the NaI-2H₂O powder (VWR chemicals, purity ≥ 99 %) was used and the temperature was increased stepwise with sufficient time in between to reach an equilibrium water vapor pressure. Based on the measured pressures, the equilibrium vapor pressure line was constructed as a function of temperature.

3.5. Microscopy of phase transitions

Two different microscopy methods were used to characterize the evolution of the morphological and structural changes of the material during and after cycling. An optical microscope (Axioplan 2) coupled to a Linkam climate chamber for temperature and relative humidity (RH) control was used for in-situ observations of NaI crystals. The samples underwent several cycles of dehydration and hydration with each cycle starting with heating to 80 $^{\circ}$ C (RH set at 0 %) with a 0.5 K/min heating rate. This temperature was held for 2 h. Then the sample was cooled to 25 $^{\circ}$ C with a 0.5 K/min heating rate and then held for 2 h with the RH set to 0 %. Finally, the RH was set to 38 %, which corresponds to 12 mbar

water vapor pressure, and held for 1.5 h to allow hydration. The RH was changed only after the temperature was stable at 25 $^{\circ}\text{C}$. Changing the temperature and RH simultaneously gives the risk of exceeding 12 mbar since the RH is temperature dependent.

Additionally, a scanning electron microscope (SEM) Phenom table top SEM was used for analysis before and after cycling. Prior to analysis, the samples were coated with a conductive gold/palladium layer using a sputter coater.

4. Results and discussions

4.1. Energy density

The DSC traces for NaBr and NaI are presented in the appendix (Fig. A1 a and b). The corresponding densities of both NaBr·2H₂O and NaI·2H₂O are given in Table 2. Here the results of our experiments are given as both gravimetric energy density (J/g) and volumetric energy density (GJ/m³). The volumetric energy density was calculated using the literature values for the density and compared with the theoretical volumetric energy densities for NaBr and NaI are in agreement with the theoretical values which confirms that both salts are suitable for heat storage in terms of energy density, when compared with the desired minimum value of 1.3 GJ/m³ [2]. Of course, in applications these values will be reduced due to the extra volume needed for vapor transport. The porous structure of the salts, allowing for improved vapor transport, will be discussed below.

4.2. Cyclability

4.2.1. NaI dihydrate

NaI shows water uptake at a water vapor pressure of 14.5 mbar with varying amounts per cycle when the heating rate is 10 K/min (and cooling rate of 10 K/min). However, it does not reach full rehydration to the dihydrate within the 6 h of hydration time in the experiment. This is illustrated in Fig. 1a. Remarkably, when the heating rate is changed to 0.1 K/min (cooling rate remains 10 K/min) the NaI does fully rehydrate into the dihydrate for at least 10 cycles as shown in Fig. 1b. This indicates that the heating rate during the dehydration step is an essential parameter in the kinetics of NaI. We will elaborate on this in the Section 4.3.

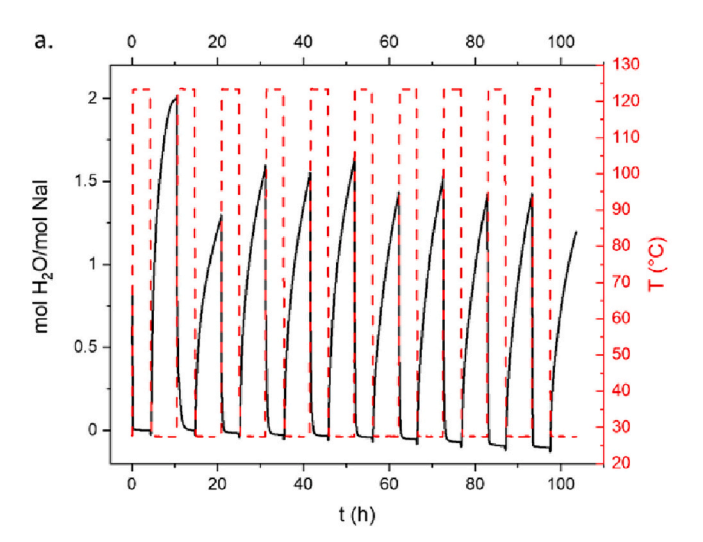
The sample cycled for 10 times with a 0.1 K/min heating rate at 14.5 mbar was reused for cycling with the same heating conditions at 12 mbar, because that is the minimum water vapor pressure in our selection criterion range for a source at 10 °C. At this water vapor pressure, the sample also fully hydrates as shown in the Appendix A2. In summary, cyclic stability of NaI is confirmed for both 14.5 and 12 mbar for at least 10 cycles between 25 °C and 130 °C, without indication of chemical degradation.

4.2.2. NaBr dihydrate

When the same experimental conditions (0.1 K/min heating at 14.5 mbar) were applied to NaBr, it showed no uptake of water at all, as detailed by the black line in Fig. 2. The absence of rehydration makes

 $\label{eq:Table 2} \begin{tabular}{ll} Table 2 \\ The measured gravimetric energy densities and the volumetric energy densities of NaBr-2H_2O and NaI-2H_2O, together with corresponding literature values for the densities. \\ \end{tabular}$

	Measured	Measured	Literature	Literature
	gravimetric	volumetric	volumetric	values
	energy density	energy density	energy density	density (g/
	(J/g)	(GJ/m ³)	(GJ/m ³) [27]	cm ³)
NaBr·2H ₂ O NaI·2H ₂ O	$710 \pm 42 \\ 604 \pm 21$	$\begin{array}{c} 1.55 \pm 0.09 \\ 1.48 \pm 0.05 \end{array}$	1.7 1.5	2.18 [31] 2.45 [32]



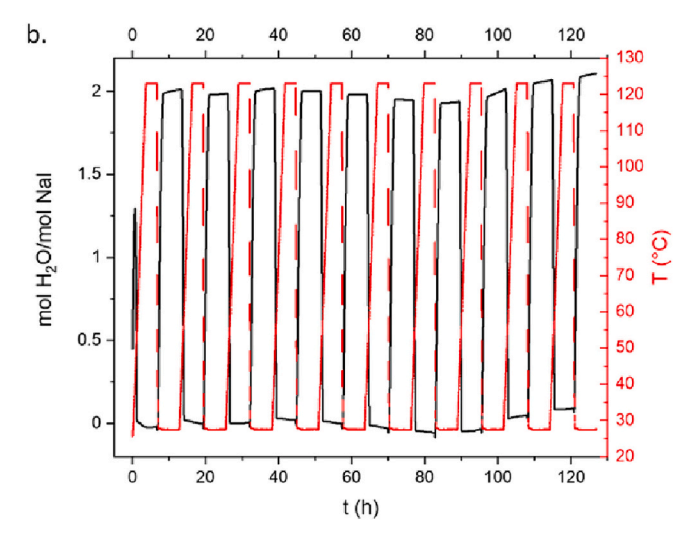


Fig. 1. The loading of NaI in moles of H_2O per mole of salt plotted versus time at 14.5 mbar for 10 cycles. The black lines indicate the loading and the red lines show the corresponding temperature profile. a. with a heating rate of 10 K/min. b. with a heating rate of 0.1 K/min. (For interpretation of the references to colour in this figure legend, the reader is referred to the web version of this article.)

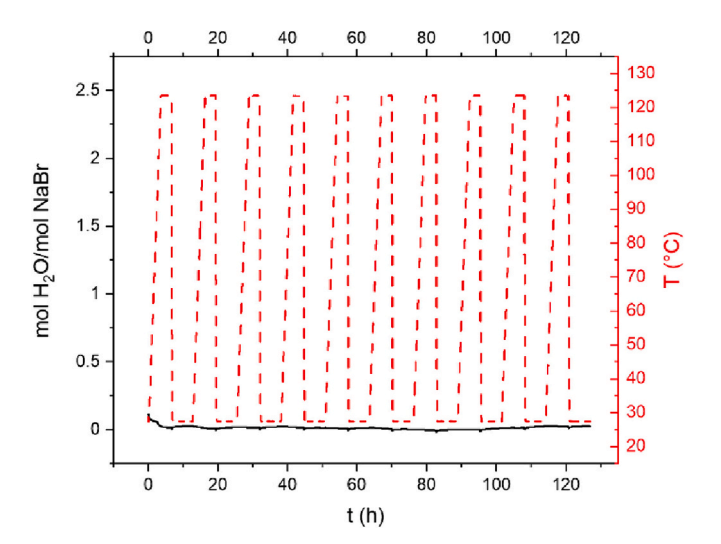


Fig. 2. Cyclability test of NaBr at 14.5 mbar with a heating rate of 0.1 K/min, the solid line shows the change in moles of water per mole of salt and the dashed line indicates the temperature profile.

NaBr unsuitable for heat storage under the conditions we have set in this research. Performing the experiment at 20 mbar water vapor pressure led to overhydration (see Appendix Fig. A 4). NaBr does thus not satisfy our criteria for cyclability.

4.3. NaI and NaBr thermodynamics, phase diagram and metastable zone

4.3.1. Dehydration enthalpy and entropy

Since both NaI and NaBr fulfil the energy density criterion, we studied their thermodynamics in further detail in order to find an explanation for the difference in cyclability of the two compounds. For NaI the measured (p,T)-values for the transition between the dihydrate and anhydrate (see Table A1 in the appendix) were used together with Eq. (4) to determine the enthalpy and entropy of transition. The resulting values are given in Table 3 together with some literature values. The experimental (both DSC and p,T) and tabulated literature values are in close agreement for the enthalpy.

For the entropy, tabulated values from Glasser and Chemnet deviate somewhat from both the experimental and other literature values

Table 3Entropy and enthalpy values for the dehydration transition per mole water.

Source	NaI•2H ₂ O		NaBr•2H ₂ O	
	$\Delta_r H^0$ [kJ/mol]	$\Delta_r S^0$ [J/mol•K]	$\Delta_r H^0$ [kJ/mol]	$\Delta_r S^0$ [J/mol•K]
DSC result	56.2 ± 2.0	-	$\textbf{50.7} \pm 2.0$	
p,T measurement	$\textbf{56.4} \pm \textbf{0.6}$	143 ± 2		
fit				
Washburn [33]	55.2	139		
Richter [34]	55.8	140	53.6	143
Glasser [27]	57.3	151	53.1	145
Chemnet [35]	55.6	151		

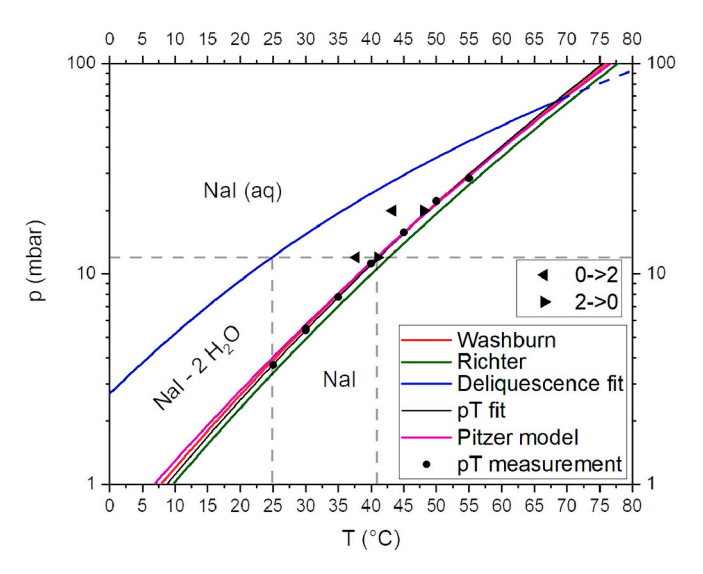


Fig. 3. NaI-H₂O phase diagram showing the phase transition lines from literature and present experimental values for the p,T equilibrium (circles) and kinetics (triangles). The deliquescence line is metastable after 68 $^{\circ}$ C, as indicated with dashes. The dashed lines are a guide to the eye for operating range at 12 mbar water vapor pressure.

(Washburn and Richter), and therefore are excluded from the phase diagram.

4.3.2. Water vapor pressure vs. temperature phase diagram

In Fig. 3, the phase diagram for the NaI-H₂O system is presented, plotted as water vapor pressure vs the temperature. Equilibrium lines for the 0–2 transition were obtained by using our present fit to the p,T data as well as enthalpy and entropy values from Washburn [33] and Richter et al. [34]. The p,T values for the 0–2 transition (filled circles) overlap with the equilibrium line from literature. The pink line was constructed by the Pitzer ion interaction model based on literature values for activity, heat, solubility and vapor pressures of NaI-H₂O systems [36]. This line also shows excellent agreement. The dashed lines in Fig. 3 are a guide to the eye for the operating window of NaI at a water vapor pressure of 12 mbar which is at temperatures between 25 °C and 42 °C.

In Fig. 4, the phase diagram for the NaBr-H $_2$ O system is presented. As the compound did not cycle, only the deliquescence line [37,38] and the hydration/dehydration equilibrium line are shown. The latter lines are based on the literature data for the dehydration enthalpy and entropy values from Richter et al. [34] and the numerical data from Dingemans [38]. The data from Glasser deviate from the latter lines. Fig. 4 makes clear why NaBr did not cycle for the conditions chosen (cycling between 25 °C and 130 °C @ 14.5 mbar). Based on the Richter data the hydration temperature at 14.5 mbar should be lower than 28 °C, which is in the lower limit boundary set for space heating. Together with the observed kinetic metastable zone width for the hydration of NaI (vide infra), the lack of cyclability is concluded to be due to a combination of thermodynamic and kinetic limitations. Therefore, NaBr was discarded for further experiments.

4.3.3. Metastability of NaI 0-2 equilibrium

Additionally, we have determined the MSZ of the 0–2 equilibrium and we found that dehydration happens at the equilibrium temperature while there is a small MSZ of 3 to 5 °C for hydration. This is indicated with the black triangles in Fig. 3. The values fit in the lower end of the range of previously reported MSZ's, which can range from a few degrees (LiCl 0–1, MgCl₂ 4–6 [30], SrCl₂ 2–6, SrCl₂ 1–2 [29]) to 10 °C or more (K_2CO_3 0–1.5, CuCl₂ 0–2 [30] or SrCl₂ 0–1 [29]). In all these examples the MSZ is symmetrical around the equilibrium, meaning that the

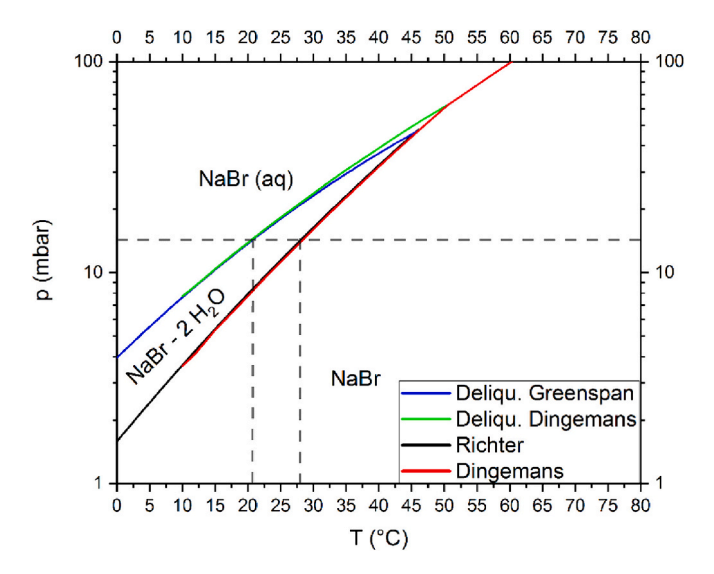


Fig. 4. NaBr-H₂O phase diagram showing the phase transition lines from literature for the p,T equilibrium. The dashed grey lines are a guide to the eye for an operating range at 14.5 mbar water vapor pressure based on the phase transition line according to Richter's data and the deliquescence line. Both these lines give rise to an incongruent melting point at 47 $^{\circ}$ C [37] or 50.5 $^{\circ}$ C [38].

hydration and dehydration transition have a similar nucleation barrier. However, for NaI, such a barrier is only found for hydration.

4.3.4. NaI deliquescence

NaI is a hygroscopic salt and has a deliquescence point of 38 % RH at 25 °C (corresponding to a water vapor pressure of 12 mbar). The blue line in Fig. 3 gives the deliquescence water vapor pressures for the whole temperature range obtained from a fit to deliquescence data from the literature [30,39–43]. The fit is valid between 0 and 68 °C and can be expressed as

$$p = 2.697915 + 0.185113 \bullet T + 0.005761 \bullet T^2 + 0.000075 \bullet T^3$$
 (5)

with p in mbar and T in °C. Deliquescence in a heat battery can cause issues with swelling and agglomeration, but on the other hand, the deliquescence transition can be used in heat storage for some salts if they are stabilized in a host matrix. However, the host matrix decreases the energy density of the salt due to the composite material volume. Examples are LiCl in vermiculite [44] or silica [45], both options resulting in a storage density of 0.6 GJ/m³ (compared to 1.8–2.0 GJ/m³ for the hydration). Another salt where the deliquescence transition is used for storage is K₂CO₃ stabilized in vermiculite. This gives an energy density of 0.9 GJ/m³ [46] (compared to 1.3 GJ/m³ for hydration). However, for NaI the deliquescence temperature at our selected water vapor pressure of 12 mbar is 25 $^{\circ}$ C, which is below the minimum of 30 $^{\circ}$ C for space heating. This means that deliquescence cannot be used for space heating. However, the hydration transition at 42 °C does fulfil the requirement for a water vapor pressure of 12 mbar. If a higher water vapor pressure is chosen, deliquescence could be considered as part of the process, NaI could be stabilized in a porous-based composite sorbent like zeolite 13X or silica gel [47]. In that case, the sorbent could be impregnated with an aqueous solution of NaI, but without exposure to light and oxygen to avoid I2-formation.

4.3.5. NaI melting

There is an intersection of the deliquescence line with the 2-0 equilibrium lines at 68 °C in the p,T - phase diagram in Fig. 3. This intersection is the incongruent melting point where the dihydrate converts to anhydrate plus a saturated aqueous solution of NaI. Fig. A5 of the appendix shows this in the alternative *T*,*x*-representation of a binary phase diagram. In a heat battery melting can occur when water vapor transport is limited, thereby locally increasing the water vapor pressure while heating during charging. This can be simulated in DSC experiments (0.1 K/min heating rate) by using either a pierced lid (limited water vapor transport possible) or a closed lid (no water vapor transport). This is shown in Fig. 5a, with the dehydration (black line) occurring for an experiment with a pierced lid and melting occurring with a closed lid (red line). The dehydration starts at approximately 40 °C and is completed at approximately 62 °C, these temperatures are marked with the dashed grey lines in Fig. 5a. The same temperatures are indicated with dashed lines in Fig. 5b, a loading vs T plot of the cyclability experiments in the TGA discussed in Section 4.2.1. This plot reveals that NaI dihydrate gradually dehydrates and dehydration is completed between these temperatures when a 0.1 K/min heating rate is applied (red line). At a higher heating rate (10 K/min), dehydration is incomplete at 68 °C so melting can occur. This transformation to the anhydrate changes the morphology of the crystals, thereby destroying previously formed pores and leads to more compact crystals. This limits water vapor transport during subsequent rehydration during discharging. Moreover, if the material melts incongruently the aqueous phases of neighboring crystals might fuse together, reducing the surface of the crystals in subsequent cycles. This incongruent melting process can be avoided by using a slow enough heating rate, which allows good water vapor transport or by avoiding temperatures >68 °C in the dehydration process. This is demonstrated in Appendix A2 where full cyclability of 10 cycles is shown when the dehydration temperature is set at 65 $^{\circ}$ C. We

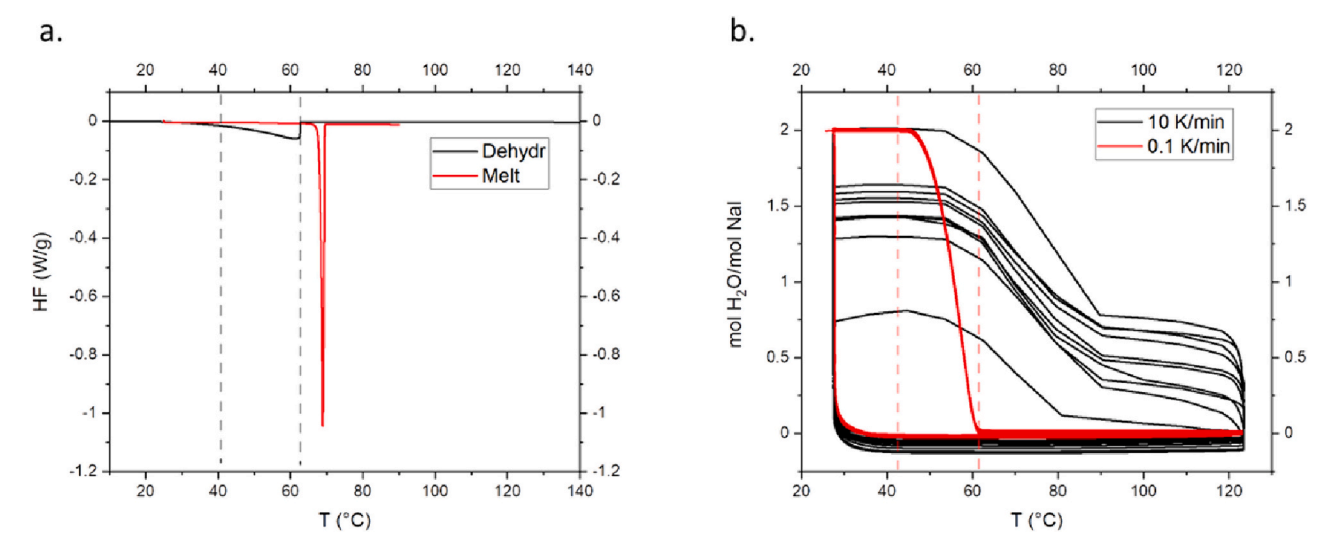


Fig. 5. a. DSC results of experiments with a 0.1 K/min heating rate with either a pierced lid (black line) or a closed lid (red line). The dashed lines are a guide to the eye for the observed start and end temperatures of dehydration for the dehydration trace. b. Cyclability experiments in TGA visualized as loading vs T with two different heating rates: 10 K/min (black lines) and 0.1 K/min (red lines). The dashed lines correspond to the ones in a. Note that the dehydration with the 0.1 K/min heating rate is completed within these dashed lines and thus before the incongruent melting point of 68 °C. (For interpretation of the references to colour in this figure legend, the reader is referred to the web version of this article.)

found that slow dehydration yields a favorable morphology and therefore investigated if this morphology is preserved in subsequent fast dehydration cycles going to a maximum temperature of 124 °C. We found, however, that pre-treating the sample with 3 slow cycles did not

prevent melting in subsequent fast cycles, which once again shows that heating above the melting temperature before dehydration is complete ruins the morphology (see Appendix A2).

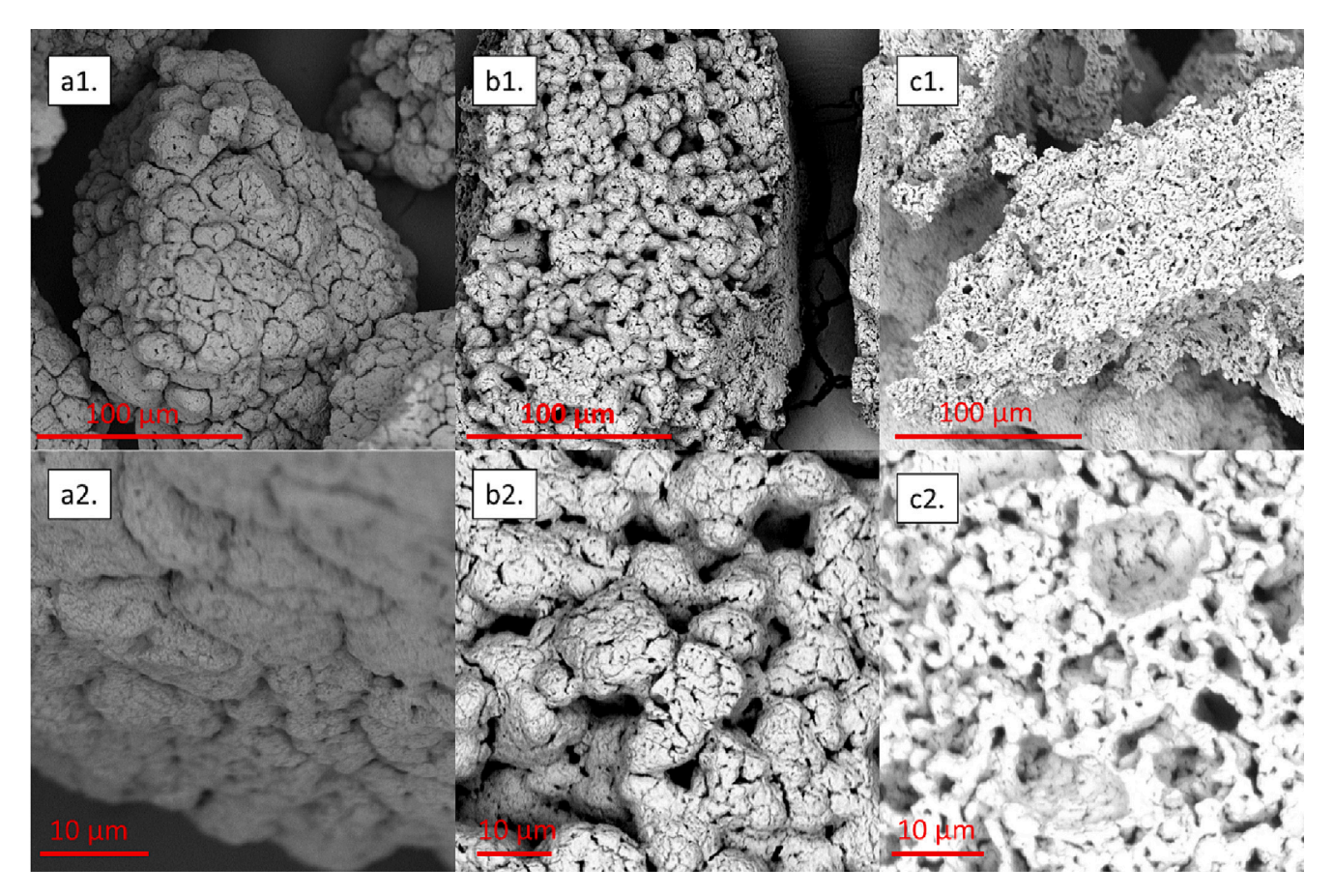


Fig. 6. SEM images of NaI with the bottom row being enlargements of the top row: a1 & a2 prior to cycling, b1 & b2 after 10 cycles of heating to 130 °C and cooling at 10 K/min to 25 °C with a constant water vapor pressure of 14.5 mbar with a 10 K/min heating rate and c1 & c2 same cyclability experiment but with a heating rate of 0.1 K/min.

4.4. NaI surface morphology

In order to understand the impact of heating rate and possible incongruent melting on the surface morphology of NaI crystals, we have studied the crystals with SEM. For that SEM images of a sample prior to cycling are compared with samples that have been cycled 10 times with heating rates of 10 K/min or 0.1 K/min. Fig. 6 a1 and a2 show a sample prior to cycling, revealing the sieved 100-150 µm NaI to consist of agglomerates of approximately 25 µm sized crystals. The crystals already show some cracks, possibly due to the sputtering process in vacuum. Cycling 10 times at a 10 K/min heating rate (Fig. 6 b1 and b2) shows the formation of additional cracks and pores leading to smaller crystallites of approximately 10 µm and more space between the separate crystallites. Finally, the 0.1 K/min heating rate (Fig. 6 c1 and c2) shows an even more porous structure where separate crystals can no longer be distinguished. This structure facilitates the water vapor transport during dehydration and hydration. These pores are probably formed during the slow dehydration step which avoids melting. The fast dehydration step of 10 K/min probably results in larger crystallites during melting, leading to recrystallization of the anhydrate from a saturated solution.

4.5. Deliquescence kinetics NaI

The standard hydration conditions for a heat battery are set at approximately 12 mbar and 25 °C. These conditions intersect with the deliquescence point of NaI of 38 % RH at 25 °C (corresponding to a water vapor pressure of 12 mbar), shown as the blue line in Fig. 3. As stated earlier, this can cause issues for operating a heat battery. However, surprisingly TGA experiments with the sample at 12 or 14.5 \pm 1.1 mbar at 27 °C gave no indication of overhydration or deliquescence within the 6 h allowed for hydration (loading did not exceed 2 mol of H₂O per mole NaI). Therefore, we have studied cycling of NaI in more detail. This was done in a humidity and temperature-controlled climate sample chamber under an optical microscope to obtain in-situ insight in the dehydration and hydration processes. For that a sample without any pre-treatment (reference) is compared with a sample that has been cycled for 10 times in TGA (0.1 K/min heating, 14.5 mbar). Both the reference sample and the pre-cycled sample were subjected to first dehydration (at 80 °C with 0 % RH) followed by hydration (at 25 °C with 38 % RH), these steps were then repeated several times. An overview of the experiment with the reference and the pre-treated samples is given in Fig. 7. The pictures at the end of the hydration step are shown below the temperature-water vapor pressure profile. The pictures of the

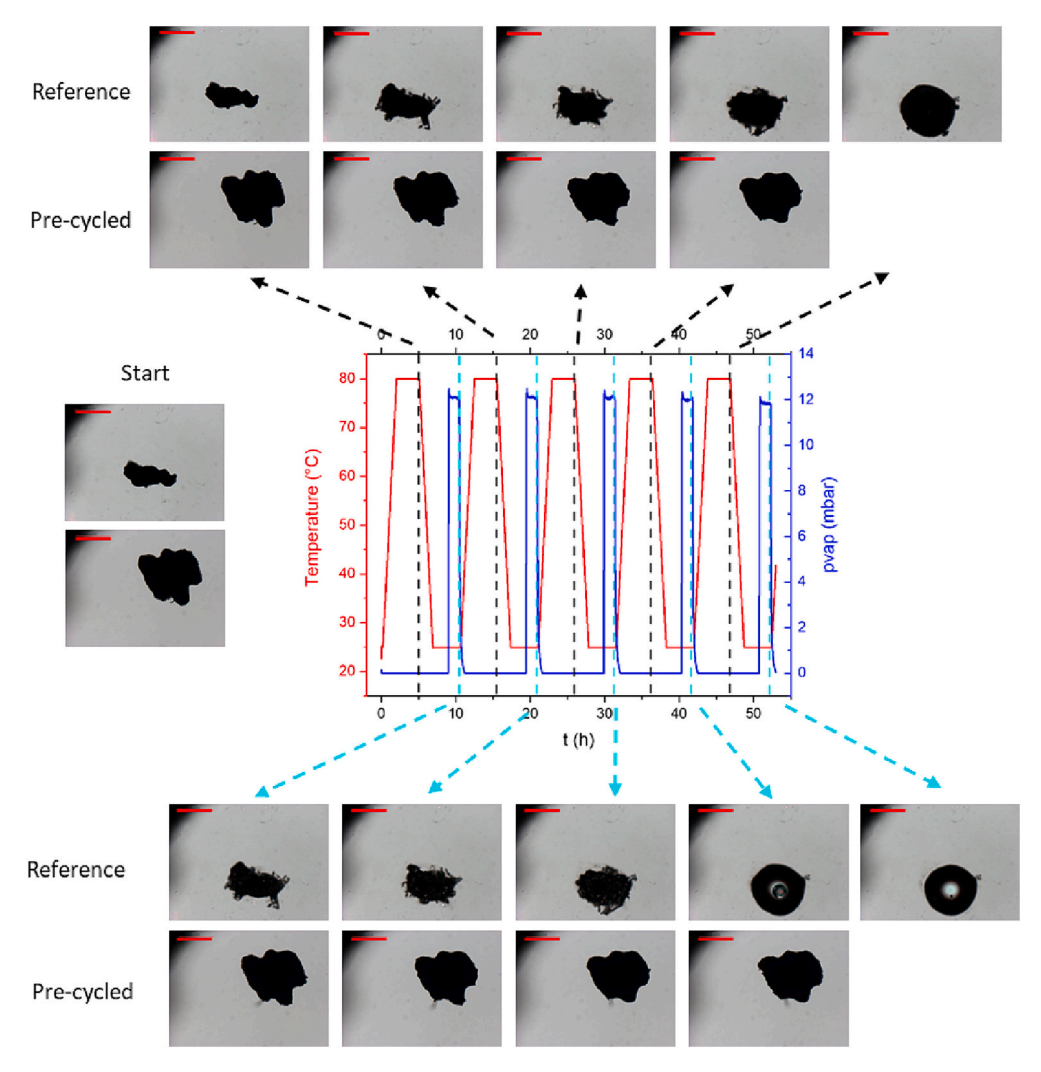


Fig. 7. Hot stage microscopy experiment of a NaI sample without pre-treatment (reference) and a pre-cycled sample. The temperature profile is shown in red and the water vapor pressure profile in dark blue. The end of each dehydration step is marked with the dashed black line and the end of each hydration step is marked with the cyan dashed line. The pictures on the left show what the samples looked like at the start of the experiment and the pictures on the top and bottom show the sample at the end of hydration or dehydration steps, indicated with the arrows. The red scalebar in the picture corresponds to 300 μm. (For interpretation of the references to colour in this figure legend, the reader is referred to the web version of this article.)

reference sample show a grain of NaI becoming gradually larger and more deformed (sharper edges) until at the 4th hydration step it appears to undergo complete deliquescence. This reveals that the deliquescence transition has slow kinetics, since it takes more than three hydration steps with 1.5 h at deliquescence conditions before any deliquescence is observed. Surprisingly, this does not occur with the pre-cycled sample. The higher porosity (see Fig. 6c) is expected to give faster kinetics, but here the porosity prevents or delays deliquescence even more. This pretreatment apparently improves the stability of the system without requiring any matrix or coating. This can explain the lack of overhydration in the TGA experiments.

5. Conclusion

An assessment of all alkali halides for heat storage showed NaI has potential as a thermochemical material in domestic space heating. NaI shows full cyclic reversibility for at least 10 cycles between 25 $^{\circ}\text{C}$ and 130 °C at both 12 and 14.5 mbar indicating it can be used for long-term heat storage in applications for heating at 25 °C. The cyclability process can be optimized by dehydrating below 68 °C to avoid melting, for example by using a low heating rate. This then results in improved stability at temperatures above 68 °C. We found that melting during the dehydration step hinders subsequent rehydration. We have determined the anhydrate to dihydrate p,T-equilibrium line which corresponds to literature data. We have also determined the metastability around this equilibrium line which is 3 to 5 °C for hydration and absent for dehydration. Therefore, melting decreases the effectiveness of the heat battery. The heat battery should be constructed such that melting is avoided and water vapor removal happens freely. Furthermore, we found that during hydration it is possible to avoid overhydration and deliquescence by pre-cycling the sample as shown in our climate-controlled

microscopy experiments. Overall, we believe NaI could be a candidate for heat storage if its high availability (and corresponding low cost) outweighs the challenges of avoiding melting and chemical degradation due to exposure to oxygen and light.

CRediT authorship contribution statement

Melian A.R. Blijlevens: Conceptualization, Data curation, Formal analysis, Investigation, Methodology, Project administration, Resources, Validation, Writing – original draft. Ekaterina D. Garina: Investigation. Quirine D.K. Wildeman: Investigation. Roy van Alst: Investigation. Natalia Mazur: Validation. Hugo Meekes: Conceptualization, Funding acquisition, Supervision, Writing – review & editing. Elias Vlieg: Conceptualization, Funding acquisition, Supervision, Writing – review & editing.

Declaration of competing interest

The authors declare that they have no known competing financial interests or personal relationships that could have appeared to influence the work reported in this paper.

Data availability

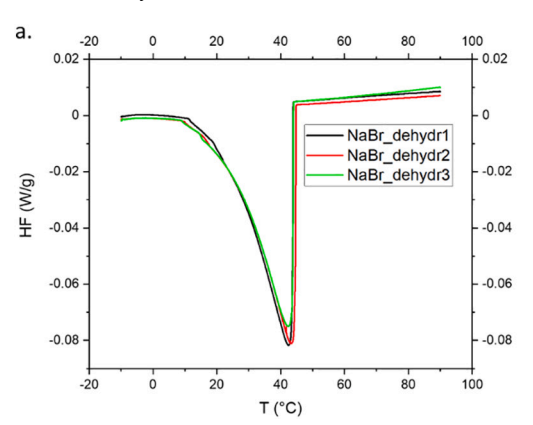
Data will be made available on request.

Acknowledgements

This publication is part of the project Mat4Heat with project number 739.017.014 of the research program Mat4Sus which is financed by the Dutch Research Council (NWO).

Appendix A. Appendix

A.1. DSC experimental results for NaBr and NaI



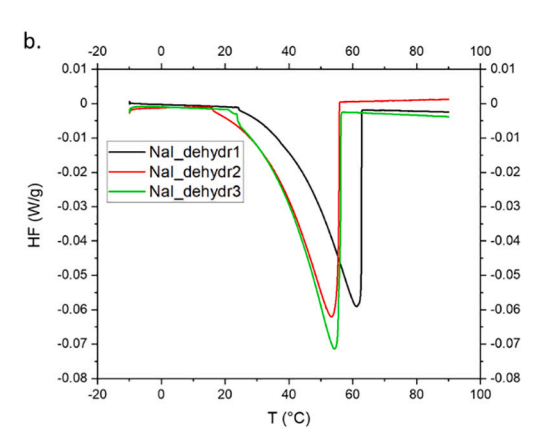


Fig. A1. DSC traces in triplo of a. NaBr and b. NaI; the heating rate was 0.1 K/min.

A.2. TGA result of NaI and NaBr cyclability experiments

The NaI sample cycled for 10 times with a 0.1 K/min heating rate at 14.5 mbar was reused in two ways, approximately 2 mg of sample was removed for SEM imaging and the rest of the sample underwent cycling with the same heating conditions but with a water vapor pressure of 12 mbar. This vapor pressure was chosen because that is the formal selection criterion. The sample also fully hydrates to the dihydrate at 12 mbar for at least 10 cycles as shown in Fig. A2 a. However, since the amount for cycling was slightly decreased it shows an increase in drift (deviation from 0). A new NaI sample was cycled for 10 times with a 10 K/min heating rate but here the dehydration temperature was set at 65 °C, as shown in Fig. A2 b. This shows full cyclic stability which proves that a heating rate of 10 K/min is not an issue as long as the temperature does not exceed the melting temperature of 68 °C.

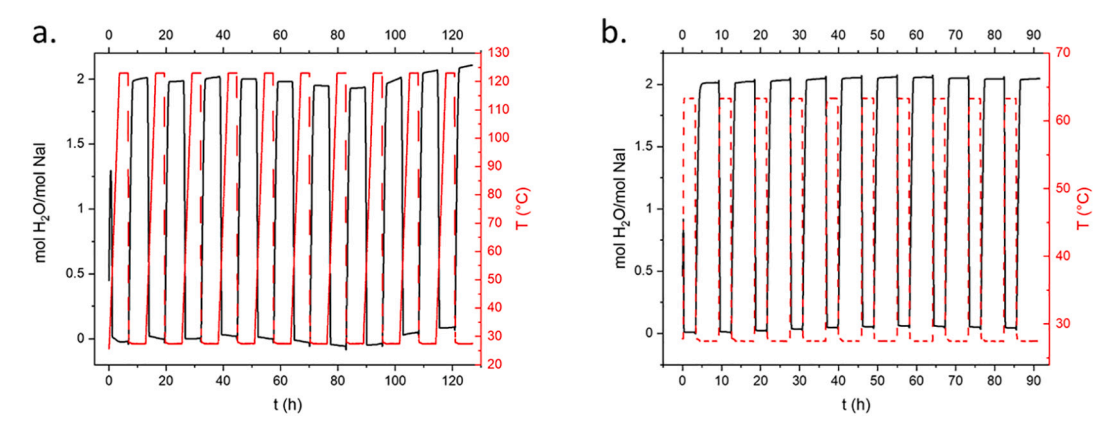


Fig. A2. The loading of NaI in moles of H_2O per mole of salt plotted versus time in an experiment with 10 cycles. The black lines indicate the loading and the red lines show the corresponding temperature profile. a. at 12 mbar with a 0.1 K/min heating rate. b. at 14.5 mbar with 10 K/min heating rate but maximum T = 65 °C. (For interpretation of the references to colour in this figure legend, the reader is referred to the web version of this article.)

We also did a cyclability experiment at 14.5 mbar with a slow (0.1 K/min) heating rate for the first 3 cycles, followed by a fast (10 K/min) heating rate for 7 cycles. The results are shown in Fig. A3. It reveals that the first 3 cycles show full cyclability but as soon as the heating rate is increased the sample does not reach full rehydration anymore. Therefore, it can be concluded that 3 cycles pretreatment does not prevent issues with incongruent melting and subsequent rehydration (see Section 4.3.5 for details on incongruent melting).

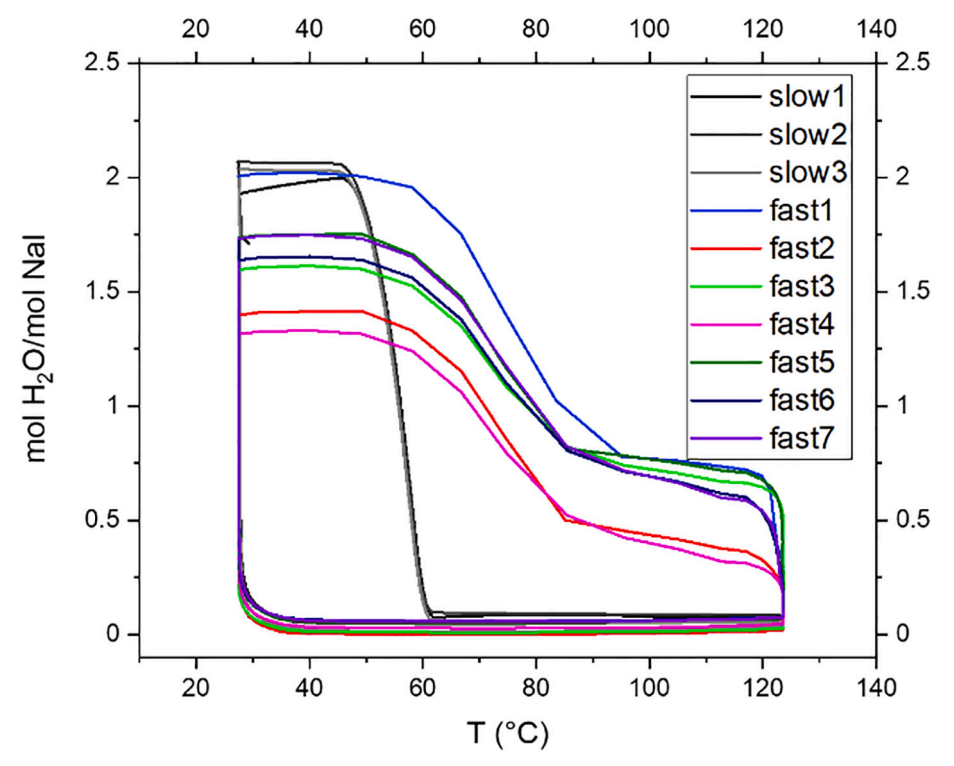


Fig. A3. Cyclability experiment of NaI with a 0.1 K/min heating rate for the first 3 cycles (grey scale), followed by 7 cycles with a 10 K/min heating rate (colours). (For interpretation of the references to colour in this figure legend, the reader is referred to the web version of this article.)

The NaBr sample was cycled for 10 times with a 0.1 K/min heating rate at 14.5 and 20 mbar shown in Fig. A4. No water uptake was observed at 14.5 mbar and at 20 mbar the water uptake exceeded the full hydration of 2 mol $\rm H_2O$ per mol of NaBr. However, no full deliquescence takes place since that would correspond to a loading of about 6 (solubility NaBr at 25 °C: 94.32 g/100 mL water).

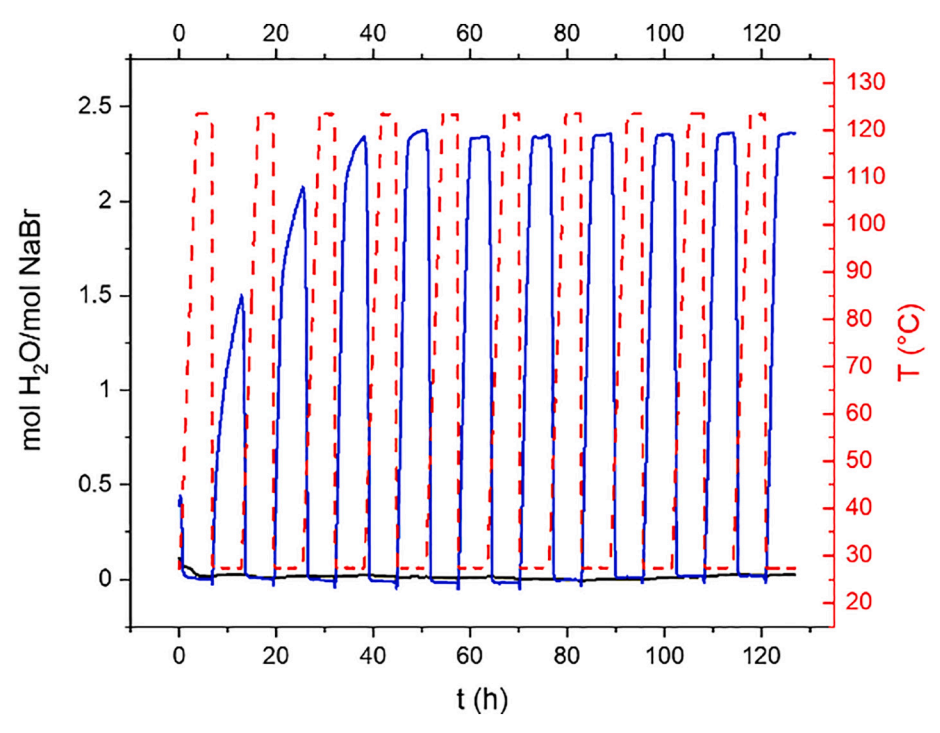


Fig. A4. Cyclability experiments of NaBr at 14.5 and 20 mbar.

A.3. Table of experimental values of NaI p,T measurement Table A1

Experimental values for p,T measurement of NaI.

T (°C)	p (mbar)	
25	3.69	
30	5.40	
30	5.49	
35	7.76	
40	11.21	
45	15.78	
50	22.23	
50	22.18	
55	28.60	

A.4. T,x phase diagram of NaI

We constructed a phase diagram of T in (°C) vs. the mole fraction X shown in Fig. A5 based on literature values for solubilities [33,48–51]. Note, the mole fraction in this figure stops at 0.5 mol NaI/mol total. In this phase diagram the boiling point elevation and freezing point depression modeled by van Alst [36] are given in respectively the bold red and blue lines. The solubilities from literature are indicated with symbols and the simulated solubilities by van Alst [36] are given with the continuous line with squares.

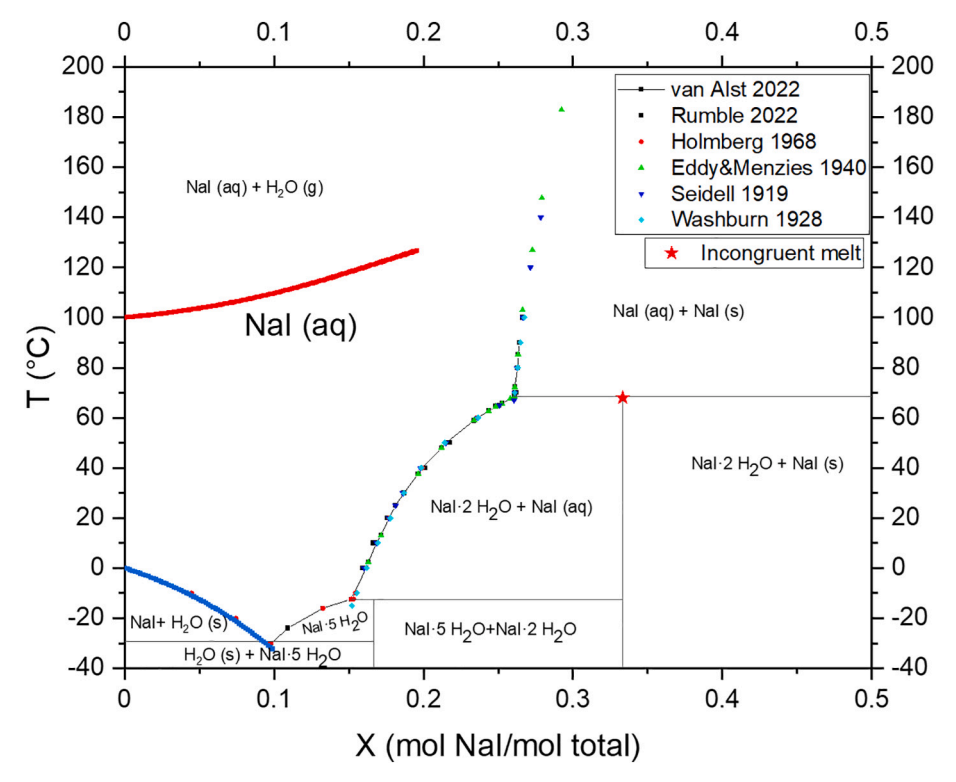


Fig. A5. T,x -phase diagram of the NaI-H₂O system (at standard atmospheric pressure of 1 bar or the saturation pressure, depending on which one is largest in that situation). The bold blue and red lines show the freezing and boiling points, respectively. (For interpretation of the references to colour in this figure legend, the reader is referred to the web version of this article.)

References

- $\label{lem:constat} \begin{tabular}{ll} Eurostat, Energy Consumption in Households. $$ $https://ec.europa.eu/eurostat/statistics-explained/index.php?title=Energy_consumption_in_households. $$ $$ $$ $$$
- [2] P.A.J. Donkers, L.C. Sogutoglu, H.P. Huinink, H.R. Fischer, O.C.G. Adan, A review of salt hydrates for seasonal heat storage in domestic applications, Appl. Energy 199 (2017) 45–68, https://doi.org/10.1016/j.apenergy.2017.04.080.
- [3] W. Li, J.J. Klemes, Q.W. Wang, M. Zeng, Salt hydrate-based gas-solid thermochemical energy storage: current progress, challenges, and perspectives, Renew. Sust. Energ. Rev. 154 (2022), https://doi.org/10.1016/j.rser.2021.111846.
- [4] K.E. N'Tsoukpoe, H. Liu, N. Le Pierres, L.G. Luo, A review on long-term sorption solar energy storage, Renew. Sust. Energ. Rev. 13 (2009) 2385–2396, https://doi. org/10.1016/j.rser.2009.05.008.
- [5] K.E. N'Tsoukpoe, F. Kuznik, A reality check on long-term thermochemical heat storage for household applications, Renew. Sust. Energ. Rev. 139 (2021), https://doi.org/10.1016/j.rser.2020.110683.
- [6] L. Scapino, H.A. Zondag, J. Van Bael, J. Diriken, C.C.M. Rindt, Energy density and storage capacity cost comparison of conceptual solid and liquid sorption seasonal heat storage systems for low-temperature space heating, Renew. Sust. Energ. Rev. 76 (2017) 1314–1331, https://doi.org/10.1016/j.rser.2017.03.101.
- [7] B. Michel, P. Neveu, N. Mazet, Comparison of closed and open thermochemical processes, for long-term thermal energy storage applications, Energy 72 (2014) 702–716, https://doi.org/10.1016/j.energy.2014.05.097.
- [8] B.W. Olesen, Radiant floor heating in theory and practice, ASHRAE J. 44 (2002) 19–26.
- [9] N. Mazur, M.A.R. Blijlevens, R. Ruliaman, H. Fischer, P. Donkers, H. Meekes, E. Vlieg, O. Adan, H. Huinink, Revisiting salt hydrate selection for domestic heat storage applications, Renew. Energy 218 (2023), https://doi.org/10.1016/j. renene.2023.119331.
- [10] W. Li, L.J. Zhang, X. Ling, Thermo-economic assessment of salt hydrate-based thermochemical heat transformer system: heat upgrade for matching domestic hot water production, Energy Convers. Manag. 277 (2023), https://doi.org/10.1016/j. enconman.2022.116644.
- [11] L.G. Gordeeva, Y.I. Aristov, Composites 'salt inside porous matrix' for adsorption heat transformation: a current state-of-the-art and new trends, Int. J. Low Carbon Technol. 7 (2012) 288–302, https://doi.org/10.1093/ijlct/cts050.
- [12] V. Brancato, L.G. Gordeeva, A.D. Grekova, A. Sapienza, S. Vasta, A. Frazzica, Y. I. Aristov, Water adsorption equilibrium and dynamics of LICL/MWCNT/PVA composite for adsorptive heat storage, Sol. Energy Mater. Sol. Cells 193 (2019) 133–140, https://doi.org/10.1016/j.solmat.2019.01.001.
- [13] E. Mastronardo, E. Piperopoulos, D. Palamara, A. Frazzica, L. Calabrese, Morphological observation of LiCl deliquescence in PDMS-based composite foams, Appl. Sci. Basel 12 (2022), https://doi.org/10.3390/app12031510.

- [14] A. Niwa, N. Kobayashi, T. Hayase, T. Fuse, Basic characteristics of heat discharge in a heat storage system using solid-liquid hydration reaction of CaCl2, CaBr2 or LiBr, Kagaku Kogaku Ronbunshu 40 (2014) 486–491, https://doi.org/10.1252/ kakoronbunshu.40.486.
- [15] I. European Commision Internal Market, Entrepreneurship and SMEs, Critical Raw Materials Resilience: Charting a Path towards greater Security and Sustainability, https://www.eesc.europa.eu/en/our-work/opinions-information-reports/opinions/critical-raw-materials-resilience-charting-path-towards-greater-security-and-sustainability.
- [16] T. Scientific, Safety Data Sheet; Potassium Fluoride. https://www.fishersci.com/store/msds?partNumber=AC390810250&productDescription=POTASSIUM+FLUO RIDE%2C+40+W+25GR&vendorId=VN00032119&countryCode=US&language=en.
- [17] T. Scientific, Safety Data Sheet; Rubidium Fluoride. https://www.fishersci.com/store/msds?partNumber=AA4714409&productDescription=RUBIDIUM+FLU ORIDE%2C+99.1%25+10G&vendorId=VN00024248&countryCode=US&language=en.
- [18] T. Scientific, Safety Data Sheet, Cesium Fluoride. https://www.fishersci.com/st ore/msds?partNumber=AC189510250&productDescription=CESIUM+FLUORIDE %2C+99%25+25GR&vendorId=VN00032119&countryCode=US&language=en.
- [19] L. Glasser, H.D.B. Jenkins, The thermodynamic solvate difference rule: solvation parameters and their use in interpretation of the role of bound solvent in condensed-phase solvates, Inorg. Chem. 46 (2007) 9768–9778, https://doi.org/ 10.1021/ic701105p.
- [20] S. Kiyabu, J.S. Lowe, A. Ahmed, D.J. Siegel, Computational screening of hydration reactions for thermal energy storage: new materials and design rules, Chem. Mater. 30 (2018) 2006–2017, https://doi.org/10.1021/acs.chemmater.7b05230.
- [21] A.A.C. Bode, P.G.M. Pulles, M. Lutz, W.J.M. Poulisse, S.F. Jiang, J.A.M. Meijer, W. J.P. van Enckevort, E. Vlieg, Sodium chloride dihydrate crystals: morphology, nucleation, growth, and inhibition, Cryst. Growth Des. 15 (2015) 3166–3174, https://doi.org/10.1021/acs.cgd.5b00061.
- [22] L.I. Grossweiner, M.S. Matheson, The kinetics of the dihalide ions from the flash photolysis of aqueous alkali halide solutions, J. Phys. Chem. 61 (1957) 1089–1095, https://doi.org/10.1021/j150554a013.
- [23] J. Jortner, R. Levine, M. Ottolenghi, G. Stein, Photochemistry of iodide ion in aqueous solution, J. Phys. Chem. 65 (1961) 1232–1238, https://doi.org/10.1021/ i100825a033.
- [24] J. Jortner, M. Ottolenghi, G. Stein, Solvent effects on photochemistry of iodide ion, J. Phys. Chem. 67 (1963) 1271–1274, https://doi.org/10.1021/j100800a026.
- [25] K. Watanabe, S. Matsuda, C.A. Cuevas, A. Saiz-Lopez, A. Yabushita, Y. Nakano, Experimental determination of the photooxidation of aqueous I- as a source of atmospheric I-2, ACS Earth Space Chem. 3 (2019) 669–679, https://doi.org/ 10.1021/acsearthspacechem.9b00007.

- [26] ICSD, ICSD Inorganic Crystal Structure Database, Leibniz Institute for Information Infrastructure, FIZ Karlsruhe, 2023.
- [27] L. Glasser, Thermodynamics of inorganic hydration and of humidity control, with an extensive database of salt hydrate pairs, J. Chem. Eng. Data 59 (2014) 526–530, https://doi.org/10.1021/je401077x.
- [28] V.S. Yungman, Thermal Constants of Substances, Wiley, 1999.
- [29] M.A.R. Blijlevens, N. Mazur, W. Kooijman, H.R. Fischer, H.P. Huinink, H. Meekes, E. Vlieg, A study of the hydration and dehydration transitions of SrCl2 hydrates for use in heat storage, Sol. Energy Mater. Sol. Cells 242 (2022), https://doi.org/ 10.1016/j.solmat.2022.111770.
- [30] L.C. Sogutoglu, M. Steiger, J. Houben, D. Biemans, H.R. Fischer, P. Donkers, H. Huinink, O.C.G. Adan, Understanding the hydration process of salts: the impact of a nucleation barrier, Cryst. Growth Des. 19 (2019) 2279–2288, https://doi.org/ 10.1021/acs.cgd.8b01908.
- [31] P. Patnaik, Handbook of Inorganic Chemicals, the McGraw-Hill Companies, Inc., United States of America, 2003.
- [32] AmericanElements, Sodium Iodide Dihydrate. https://www.americanelements. com/sodium-iodide-dihydrate-13517-06-1#section-about.
- [33] E.W. Washburn, International Critical Tables of Numerical Data, Physics, Chemistry and Technology, 2003.
- [34] M. Richter, E.M. Habermann, E. Siebecke, M. Linder, A systematic screening of salt hydrates as materials for a thermochemical heat transformer, Thermochim. Acta 659 (2018) 136–150, https://doi.org/10.1016/j.tca.2017.06.011.
- [35] MoscowStateUniversity, Chemnet. http://www.chem.msu.ru/cgi-bin/tkv.pl?bru tto=H2O&show=search&joules=0.
- [36] R. van Alst, Construction of Phase Diagrams of the NaI H₂O system, using a Pitzer Ion Interaction Approach, (Institute for Molecules and Materials), available from e.vlie g@science.ru.nl.
- [37] L. Greenspan, Humidity fixed-points of binary saturated aqueous-solutions, J. Res. Natl. Bur. Stand. 81 (1977) 89–96, https://doi.org/10.6028/jres.081A.011.
- [38] P. Dingemans, The vapour pressure of solutions saturated with lead nitrate and ammonium nitrate, J. R. Neth. Chem. Soc. 64 (1945) 199–204.

- [39] D.T. Acheson, Vapor pressures of saturated aqueous salt solutions, Humidity and Moisture 3 (1965) 521–530.
- [40] J.N. Brönsted, Studien zur chemischen affinität. VIII. Kristallinische Umwandlungen der Alkalisalze, Z. Phys. Chem. 82 (1913) 621–640.
- [41] D.S. Carr, B.L. Harris, Solutions for maintaining constant relative humidity, Ind. Eng. Chem. 41 (1949) 2014–2015.
- [42] C.P. Hedlin, F.N. Trofimenkoff, Relative humidities over saturated solutions of nine salts in the temperature range from 0° to 90° F, in: International Symposium on Humidity and Moisture, Reinhold Publishing Corporation, Washington DC, 1963, pp. 519–520.
- [43] G.M. Richardson, R.S. Malthus, Salt for static control of humidity at relatively low levels, J. Appl. Chem. 5 (1955) 557–567.
- [44] Y.N. Zhang, R.H. Wang, T.X. Li, Y.J. Zhao, Thermochemical characterizations of novel vermiculite-LiCl composite sorbents for low-temperature heat storage, Energies 9 (2016), https://doi.org/10.3390/en9100854.
- [45] N. Yu, R.Z. Wang, Z.S. Lu, L.W. Wang, Development and characterization of silica gel–LiCl composite sorbents for thermal energy storage, Chem. Eng. Sci. 111 (2014) 73–84, https://doi.org/10.1016/j.ces.2014.02.012.
- [46] A.I. Shkatulov, J. Houben, H. Fischer, H.P. Huinink, Stabilization of K2CO3 in vermiculite for thermochemical energy storage, Renew. Energy 150 (2020) 990–1000, https://doi.org/10.1016/j.renene.2019.11.119.
- [47] W.S. Hua, H.F. Yan, X.L. Zhang, X.D. Xu, L.Y. Zhang, Y. Shi, Review of salt hydrates-based thermochemical adsorption thermal storage technologies, J. Energy Storage 56 (2022) 106158, https://doi.org/10.1016/j.est.2022.106158.
- [48] R.D. Eddy, W.C. Menzies, The solubilities of certain inorganic compounds in ordinary water and in deuterium water, J. Phys. Chem. 44 (1940) 207–235.
- [49] K.E. Holmberg, Phase Diagrams of Some Sodium and Potassium Salts in Light and Heavy Water, AktieBolaget Atomenergi, (Stockholm, Sweden, 1968.
- [50] J.R. Rumble, Handbook of Chemistry and Physics Internet Version 2005, 100 ed., CRC Press, Boca Raton, FL, 2005.
- [51] A. Seidell, Solubilities of Inorganic and Organic Compounds, 2nd ed., D. van Nostrand Company, New York, 1919.